Science Advances
AAAS

advances.sciencemag.org/cgi/content/full/7/24/eabf7460/DC1

Supplementary Materials for

Global tropospheric ozone responses to reduced NO_x emissions linked to the COVID-19 worldwide lockdowns

Kazuyuki Miyazaki*, Kevin Bowman, Takashi Sekiya, Masayuki Takigawa, Jessica L. Neu, Kengo Sudo, Greg Osterman, Henk Eskes

*Corresponding author. Email: kazuyuki.miyazaki@jpl.nasa.gov

Published 9 June 2021, *Sci. Adv.* **7**, eabf7460 (2021)
DOI: 10.1126/sciadv.abf7460

The PDF file includes:

Other Supplementary Material for this manuscript includes the following:

(available at advances.sciencemag.org/cgi/content/full/7/24/eabf7460/DC1)

Supplementary Materials and Methods

In this section, we provide information on the validation of the data assimilation and model results against satellite NO_2 measurements (section S1), ozonesonde measurements (section S2), satellite ozone measurements from CrIS (section S3), and surface measurements from OpenAQ (section S4).

S-1. Comparisons against satellite NO_2 measurements

Data assimilation improved the agreement between the model and the assimilated TROPOMI NO_2 retrievals. After data assimilation, the global monthly mean root-mean-square-error (RMSE) of the model relative to TROPOMI is reduced from 0.59-1.08 $\times 10^{15}\, molec\, cm^{-2}$ to 0.15-0.22 $\times 10^{15}\, molec\, cm^{-2}$, whereas the spatial correlations are improved from 0.74-0.86 to 0.94-0.96 during February-July 2020. The temporal variations of regional mean NO_2 columns are also well-reproduced by data assimilation for major polluted regions (Fig. S1), whereas the model simulation with the a priori emissions overestimated tropospheric NO_2 columns over East China and underestimated them over Australia, southeast Asia, and the Middle East. The temporal correlations between the modeled and measured regional mean NO_2 columns are improved by 0.10-0.33 for all major polluted areas, whereas the RMSEs are reduced by about 10-80 %. The improved agreement confirms that the observational constraints were sufficient to reproduce the observed variability of NO_2 globally through emission optimization. Nevertheless, the inadequacies of the improvements in simulated tropospheric NO_2 columns for instance over South Africa could be related to the small number of observations, large observation errors for highly polluted cases, and model biases in the NOx chemical lifetime. The remaining error may indicate a possible bias in the estimated emissions.

S-2. Ozonesonde measurements

We use global ozonesonde observations taken from the World Ozone and Ultraviolet Radiation Data Center (WOUDC) database (available at `http://www.woudc.org`) to validate our simulated vertical ozone profiles. The bias in TCR-2 reanalysis ozone relative to the ozonesonde measurements is less than 1.2 ppb in the lower troposphere, except for the tropics, and less than 3.1 ppb in the middle and upper troposphere, except for the SH high latitudes. Temporal correlations are greater than 0.85 for most regions for 2005-2018 (*20*). We confirm a similar data assimilation performance for 2020 against the ozonesonde observations, but with many fewer observations available at the time of this research. The validation against ozonesonde observations for the COVID time period will be extended in a follow-on study.

S-3. Satellite ozone measurements from CrIS

We use the CrIS version 1.8 L2 tropospheric ozone profile product to evaluate the global distribution of tropospheric ozone. The ozone profile retrievals were performed using the JPL MUlti-SpEctra, MUlti-SpEcies, Multi-Sensors (MUSES) algorithm (*70*) on CrIS level 1B (L1B) spectral radiances. Preliminary validation of the CrIS ozone products against ozonesonde measurements shows similar performance to ozone retrievals from the Tropospheric Emission Spectrometer in the lower troposphere, with mean biases of less than 20 % at mid-latitudes of both hemispheres (*71*). In many cases, CrIS ozone shows reduced noise compared to ozone from TES. The mean uncertainty of TES retrievals (i.e., random errors) averaged over three months typically ranges from 2 to 4 ppbv at 700 hPa at low and mid latitudes globally, whereas the CrIS provide reduced noise than TES. The observed differences between 2020 and 2018-2019 from CrIS (ranging from 4 to 7 ppb) are thus considered to be meaningful over most of polluted areas.

Fig. S3 shows global maps of monthly mean ozone concentrations at 700 hPa from CrIS, the model using a priori emissions, and data assimilation. The CrIS averaging kernels have been applied to the model output. The CrIS retrievals provide detailed spatial patterns in ozone around the world. The data assimilation fields well capture the observed spatial and temporal changes in tropospheric ozone from February to June 2020. In contrast, the model simulation with a priori emissions generally overestimates lower tropospheric ozone in the NH extratropics and underestimates it in the tropics and subtropics of both hemispheres. The data assimilation removes most of the model biases, with RMSE reduced from 8.0-9.3 ppb to 4.3-7.5 ppb, and increases the spatial correlation from 0.83-0.89 to 0.86-0.93 for the globe. At regional scale, both mean bias and RMSE (in brackets) are reduced by 37-73% (31-67%) over East Asia (80–125°E, 20–45°N) except in February, 25-42% (15-33%) over Europe (10°W–30°E, 35–60°N) except from April through June, 8-47% (14-38%) over North America (70–125°W, 28–50°N), 9% (12%) over South America (35–80°W, 40°S–10°N) except from March through June, 95-99% (32-56%) over Africa (20°W–40°E, 30°S–20°N) except in February, and 45-76% (37-40%) over Australia (110–155°E, 10–41°S) except from March through May. The relatively large remaining biases over central South America, which may be associated with remaining model errors in processes involved in active ozone production related to fires in the Amazon region, and those in the NH subtropics need to be explored further. The improved agreement demonstrates that the simultaneous optimization of concentration and emissions from multi-constituent data assimilation is an efficient method to correct the global tropospheric ozone distribution.

The CrIS ozone retrievals were also used to evaluate our modeled COVID ozone anomaly (Fig. 6a). The model with the COVID emissions shows improved agreement with the CrIS observations relative to the model with BAU emissions, especially before March for China and after April for other polluted regions. These results provide important information on the

performance of our COVID NOx emission anomaly and its tropospheric ozone response.

S-4. Surface measurements from OpenAQ

The surface ozone measurements in 1,906 cities were downloaded from the OpenAQ platform via Amazon Athena and were used to evaluate surface ozone changes worldwide (OpenAQ, 2020; `http://openaq.org/`, accessed 13 Oct., 2020). The OpenAQ data have already been used in previous studies to quantify changes in surface ozone concentrations during the COVID-19 pandemic (*11*). The OpenAQ data in South Asia, including India, were excluded from our analysis due to data quality issues. The evaluation of sensors used for the United States Environmental Protection Agency (EPA) network is summarized at `https://www.epa.gov/air-sensor-toolbox/evaluation-emerging-air-sensor-performance`.

Using the OpenAQ surface ozone observations, we evaluate the simulated surface ozone for both the BAU and COVID-19 emissions scenarios. As shown in Fig. S4 for May 2020, both of the model simulations capture the observed spatial pattern of surface ozone. The validation results for each month during February-June 2020 are summarized in Table S1 and shown in Fig. 6b. The agreement against the 2020 surface observations is improved for polluted regions such as North America, Europe, the Middle East, and East Asia when using the COVID-19 emissions. The improvement is obvious after April except for China, with bias (RMSE) reductions of 22-26 (6-16) % for the USA, 11-20 (6-14) % for Europe, and 25-28 (12-23) % for the Middle East. For China, the error reductions are larger for February and May (13-33 (7-18) %), corresponding to the early lockdown. The agreement against NO_2 surface observations is also improved, with RMSE reductions of 3-24 % for the USA (except for February), 4-27 % for Europe, and 2-19 % for the Middle East (except for February), and 5-40 % for East Asia. The reported negative bias in the TROPOMI NO_2 measurements (*71*) could explain the remaining negative NO_2 bias.

The COVID emissions scenario also improves the simulated temporal evolution of surface ozone. As shown in Fig. S5, the temporal changes in ozone (in ppb per month) during the analysis period are overall consistent between the model and the OpenAQ observations, with improved agreement in the COVID-19 scenario shown by increases in the spatial correlation coefficient of 0.024-0.046 and reduction of RMSE by 13-30 %. In addition, the improved performance of the COVID-19 emissions can be seen in the reduced linear regression intercept from 3.38 to 2.35 in April-May and from 2.45 to 1.92 in May-June. For individual stations, the model has relatively large uncertainty. The positive bias of the simulated surface ozone in May and June could be attributed to model errors such as excessive vertical mixing and underestimated NOx-titration over urban areas associated with the low model resolution (*72*). These will further be explored in a follow-on study.

Table S1. Comparisons of modeled surface ozone and NO_2 concentrations against the surface measurements from the OpenAQ platform over North America, Europe, the Middle East, and eastern Asia. The monthly RMSEs and biases (in ppb) are shown for the model simulations using the COVID-19 emissions and the BAU emissions (in parentheses) during February-June 2020.

	Ozone RMSE (ppb)					NO_2 RMSE (ppb)				
	Feb	Mar	Apr	May	Jun	Feb	Mar	Apr	May	Jun
N America	9.7	11.0	10.9	13.7	15.3	8.8	6.6	5.2	4.5	3.9
	(9.8)	(11.2)	(11.6)	(15.7)	(18.2)	(8.5)	(6.8)	(6.0)	(5.3)	(5.1)
Europe	8.2	9.1	10.3	12.7	16.6	7.4	7.1	5.7	5.1	4.5
	(8.2)	(9.1)	(10.9)	(14.9)	(19.3)	(7.7)	(7.4)	(6.6)	(6.3)	(6.2)
Middle East	9.8	9.2	8.9	12.2	13.9	8.7	5.9	3.8	4.2	4.0
	(9.9)	(9.9)	(10.1)	(15.8)	(16.4)	(8.6)	(6.0)	(4.3)	(5.2)	(4.8)
E Asia	16.7	17.9	25.2	27.9	31.1	11.9	10.8	11.7	9.5	7.7
	(20.2)	(19.3)	(25.4)	(28.6)	(31.4)	(20.1)	(12.5)	(12.3)	(10.3)	(8.5)
	Ozone bias (ppb)					NO_2 bias (ppb)				
	Feb	Mar	Apr	May	Jun	Feb	Mar	Apr	May	Jun
N America	0.1	4.9	3.9	8.1	10.8	-3.4	-1.0	-0.5	-0.6	0.3
	(-0.4)	(5.0)	(5.2)	(10.5)	(14.0)	(-2.6)	(0.2)	(0.9)	(0.6)	(1.5)
Europe	3.2	4.5	6.0	10.6	15.7	-2.9	-2.4	-1.4	-1.0	-0.4
	(3.0)	(4.0)	(7.0)	(12.0)	(19.8)	(-2.2)	(-1.4)	(0.3)	(0.5)	(0.7)
Middle East	0.7	4.7	5.6	11.2	13.3	-1.6	-0.6	-0.1	-0.5	-0.0
	(0.5)	(5.4)	(7.8)	(14.9)	(17.8)	(-1.2)	(-0.5)	(0.2)	(0.1)	(0.2)
E Asia	-11.5	-12.2	-20.2	-16.7	-14.9	5.5	-1.7	-2.3	-3.1	-2.8
	(-17.3)	(-14.0)	(-20.5)	(-18.1)	(-15.3)	(11.8)	(1.2)	(-2.2)	(-2.6)	(-1.0)

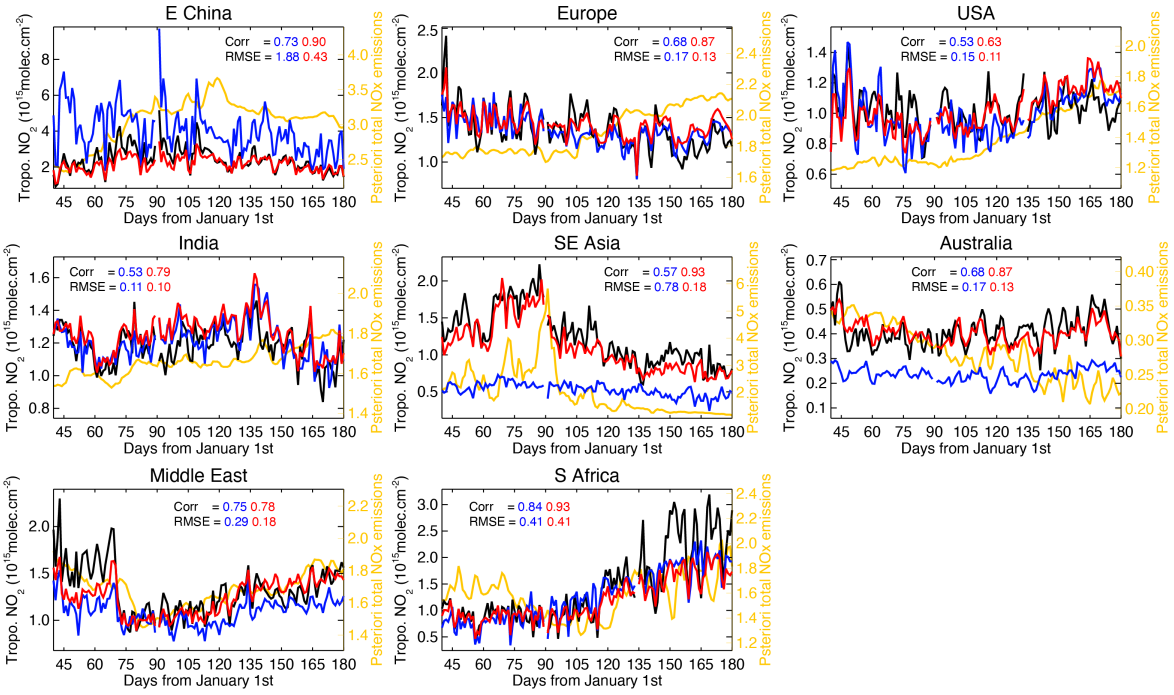

Fig. S1. Time series of regional monthly mean tropospheric NO_2 columns (in $10^{15}\ molec\,cm^{-2}$) averaged over China (110–123°E, 30–40°N), Europe (10°W–30°E, 35–60°N), the United States (70–125°W, 28–50°N), India (68–89°E, 8–33°N), Southeast Asia (96–105°E, 10–20°N), Australia (113–155°E, 11–44°S), the Middle East (37–55°E, 23–38°N), and Southern Africa (25–34°E, 22–31°S) obtained from the TROPOMI observations (black), control run using a priori emissions (blue), and the data assimilation (red). The temporal correlation and RMSE values are shown in each figure. The a posteriori total (anthropogenic, biomass burning, and soil) NOx emissions obtained from the TROPOMI NO_2 data assimilation averaged over the same areas are also shown (orange, in $10^{-11} kgNm^{-2}s^{-1}$).

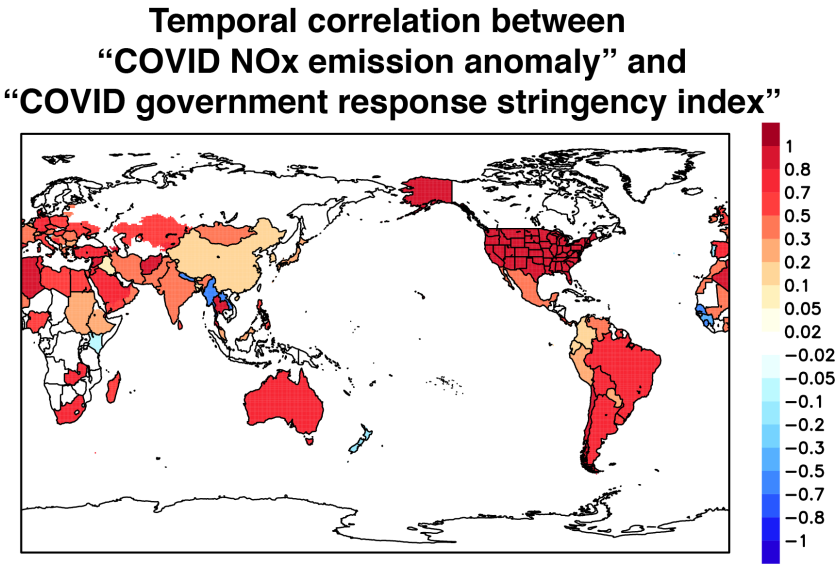

Fig. S2. Global map of temporal correlations between the COVID NOx emission anomaly and the COVID-19 government response stringency index during March-June 2020.

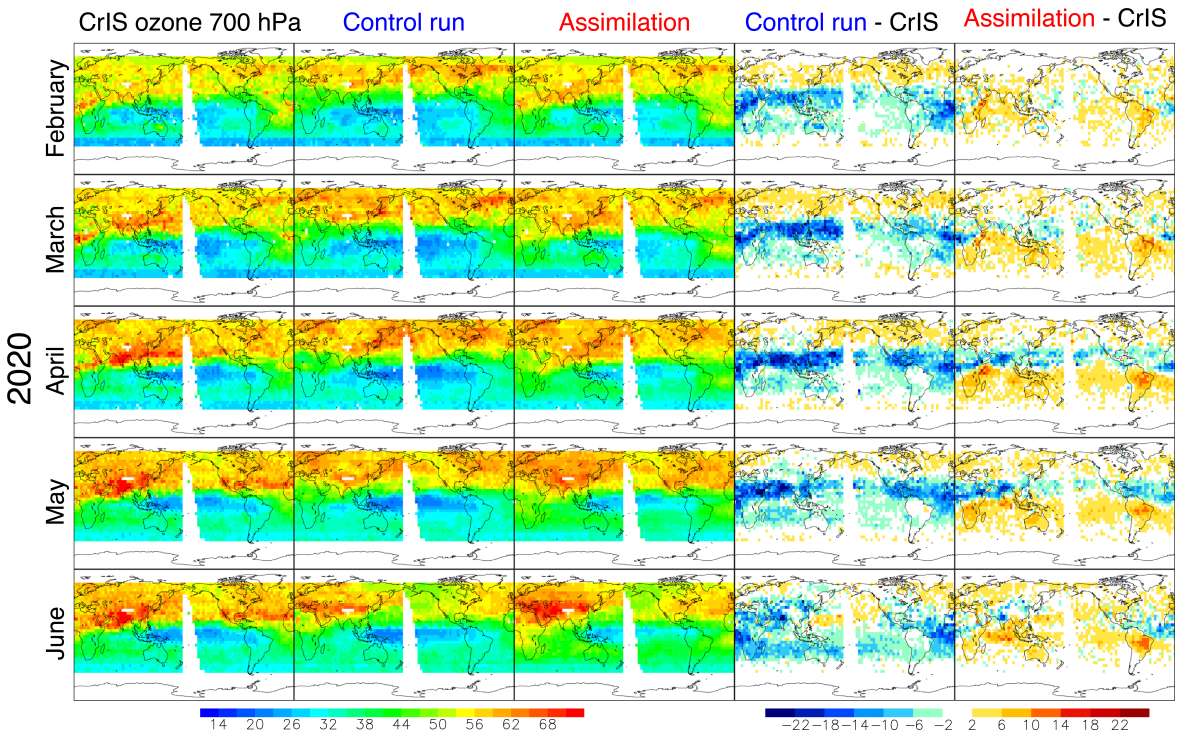

Fig. S3. Global distributions of monthly mean ozone concentration (in ppb) at 700 hPa for February to June 2020 (from top to bottom) from the CrIS satellite retrievals (left column), control run using a priori emissions (2nd left column), and data assimilation run (3rd left column). Also shown is the difference between the control run and the satellite retrievals (4th left column), and the difference between the data assimilation run and the satellite retrievals (right column).

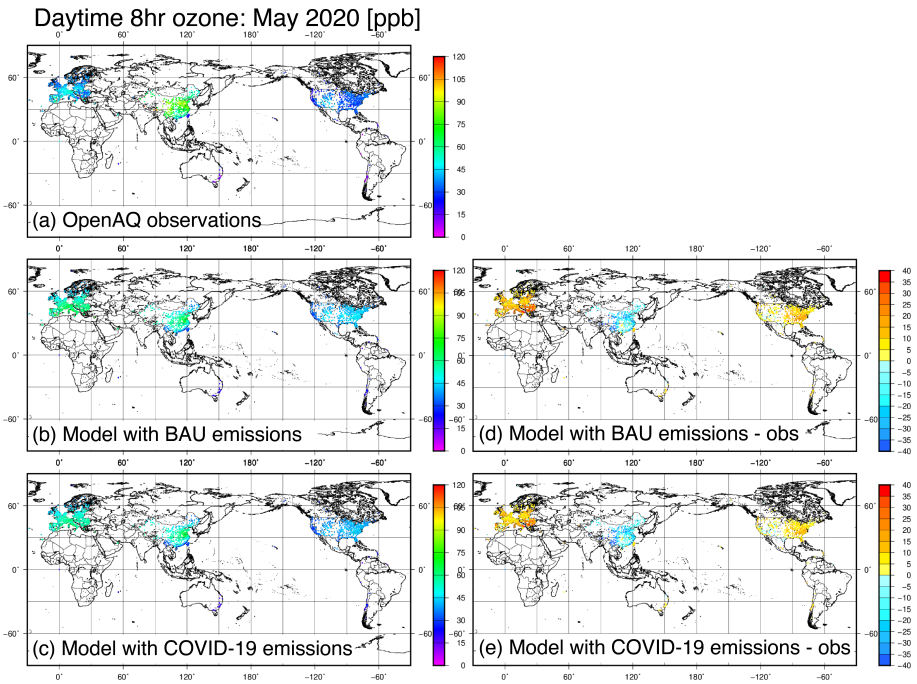

Fig. S4. Global maps of monthly mean daytime 8-hour average surface ozone concentrations in May 2020 from (a) the OpenAQ observations, (b) the model simulation with the BAU emissions, (c) the model simulation with the COVID-19 emissions, (d) difference between the model simulation with the BAU emissions and the observations (b-a), and (e) the model simulation with the COVID-19 emissions and the observations (c-a). The statistics are summarized in Table S1.

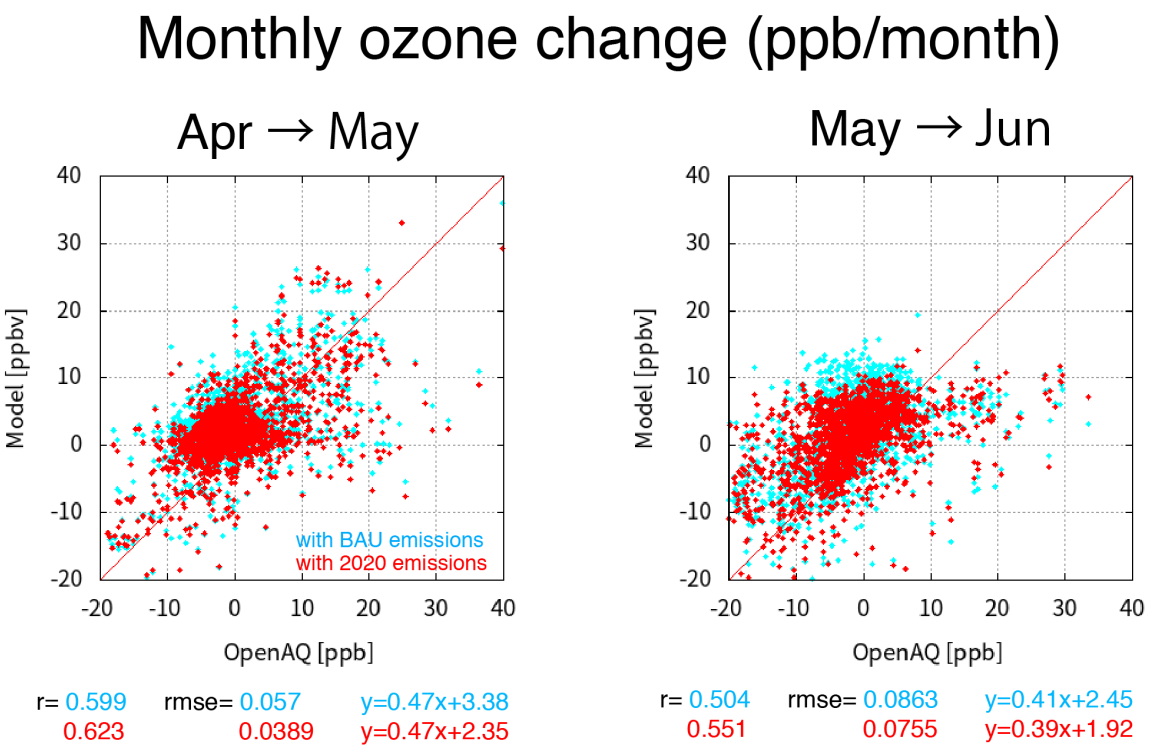

Fig. S5. Scatter plots of temporal changes in surface ozone (ppb/month) between the OpenAQ observations and model simulation with the BAU emissions (light blue) and between the OpenAQ observations and model simulation with the COVID-19 emissions (red) for April to May (left) and May to June (right) in 2020.

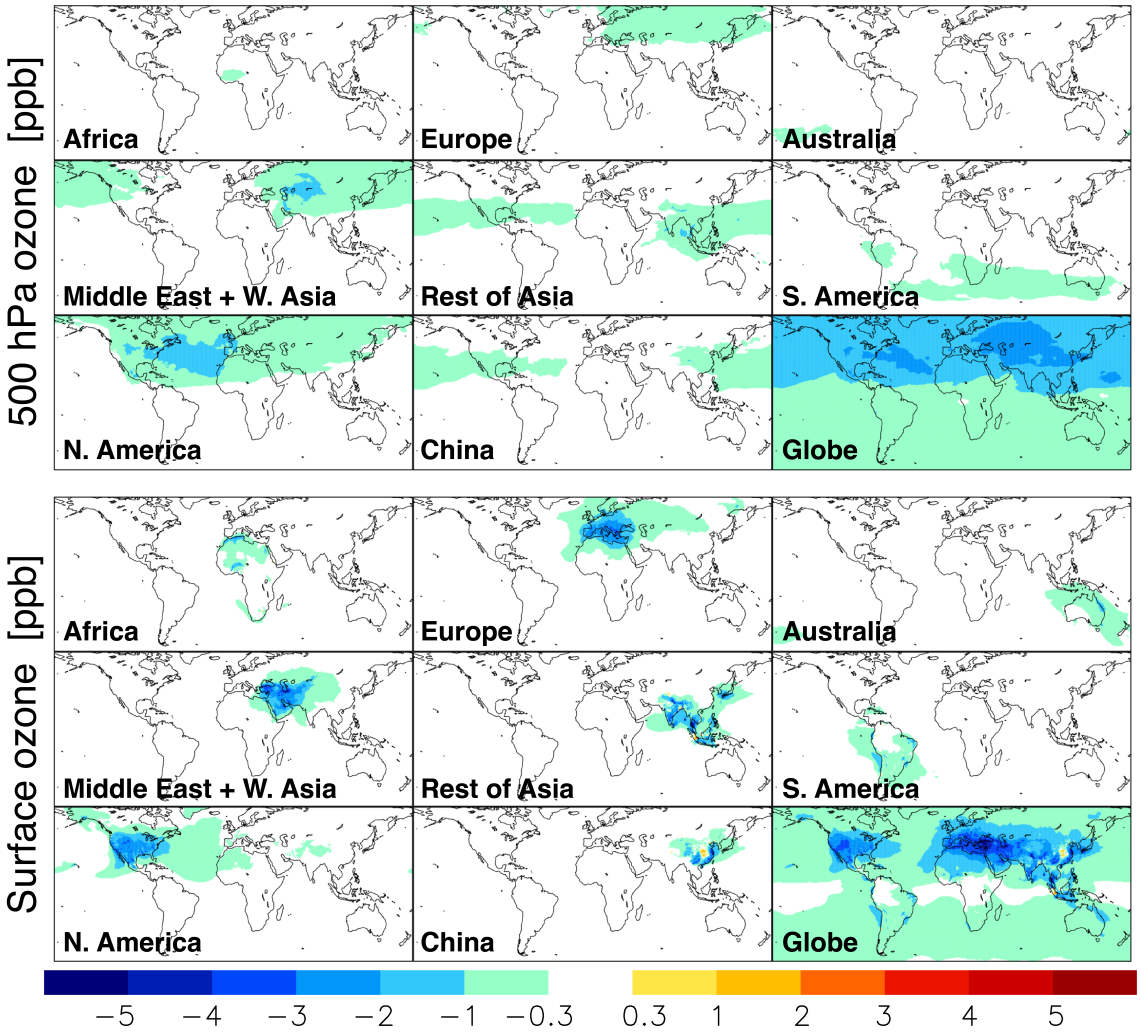

Fig. S6. Spatial distributions of the simulated ozone response (in ppb) at the surface (lower panels) and 500 hPa (upper panels) using the COVID-19 NOx emission anomaly for each region and for the globe in May 2020.

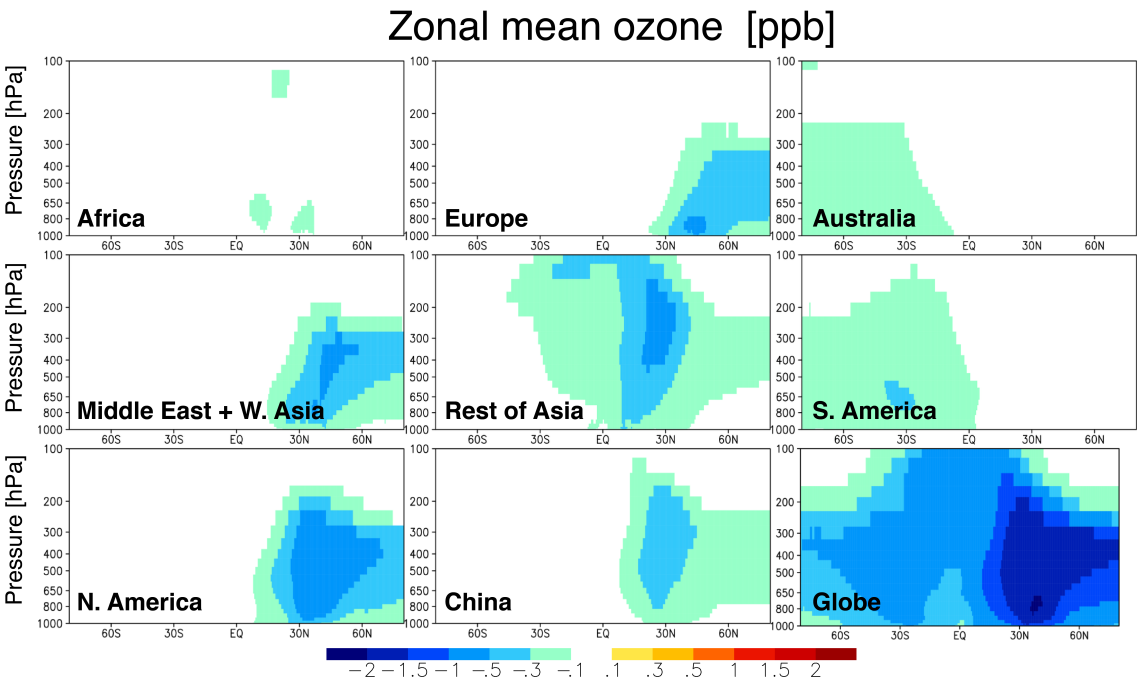

Fig. S7. Same as in Fig. S6, but for the latitude-pressure cross-section of zonal mean ozone changes.

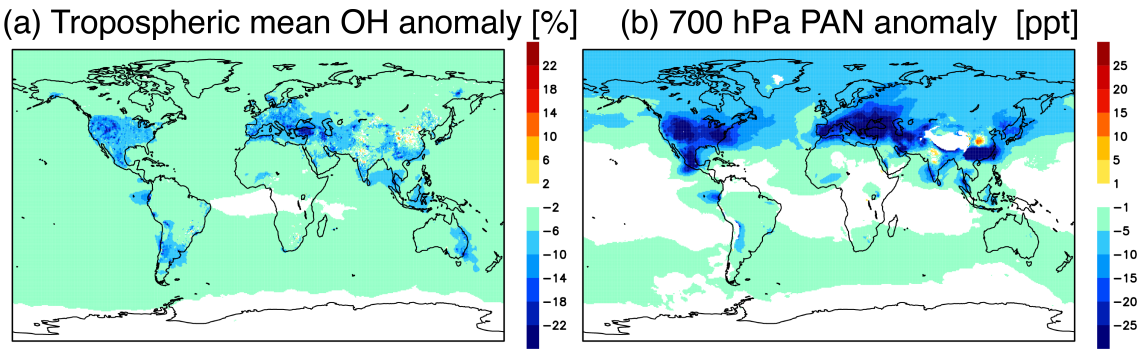

Fig. S8. Global maps of the simulated changes in (a) tropospheric mean OH concentrations (in %) and (b) PAN concentrations at 700 hPa (in ppt) for May 2020 due to the COVID-19 NOx emission anomaly.

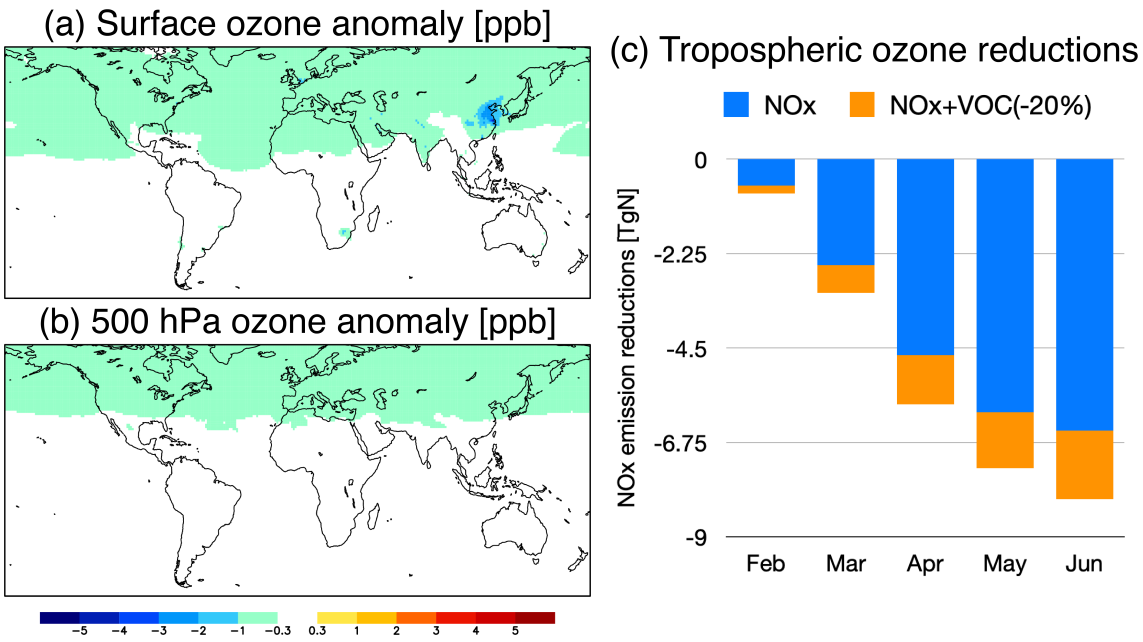

Fig. S9. (a, b) Same as in Fig. S6, but for the simulated ozone response (in ppb) in May 2020 to 20 % reductions of anthropogenic VOC (C_2H_6, C_3H_8, ONMV, C_2H_4, C_3H_6, CH_3OH, CH_3COCH_3) emissions for the globe from February through May 2020 in the 2020 emission scenario where the COVID NOx emissions are used. (c) Decrease in the global tropospheric ozone burden (in TgO_3) due to the COVID NOx emission reductions (blue) and additional global anthropogenic VOC emission reductions of 20 % (orange).